THE JOURNAL OF PHYSICAL CHEMISTRY A

Article

pubs.acs.org/JPCA

A First-Principles Approach to the Dynamics and Electronic Properties of *p*-Nitroaniline in Water

Benedito J. Costa Cabral,*[,†] Kaline Coutinho,[‡] and Sylvio Canuto[‡]

[†]Departamento de Química e Bioquímica and Grupo de Física Matemática da Universidade de Lisboa, Faculdade de Ciências da Universidade de Lisboa, Campo Grande 1749-016 Lisboa, Portugal

[‡]Instituto de Física da Universidade de São Paulo, 05508-090 Cidade Universitária, São Paulo, São Paulo Brazil

ABSTRACT: Born−Oppenheimer molecular dynamics of *p*-nitroaniline (PNA) in water was carried out and the electronic structure was investigated by time-dependent density functional theory. Hydrogen bonding involving the PNA nitro and amine groups and the water molecules leads to an ∼160 cm^{-1} red shift of the ν(N—O) and ν(N—H) stretching frequencies relative to the gas phase species. Our estimate for the peak position of the charge transfer (CT) band in the absorption spectrum of PNA in water (∼3.5 eV) is in good agreement with experimental data (3.3 eV). We have investigated the specific role played by local hydrogen bonding and electrostatic interactions on the electronic absorption spectrum. It is shown that although electrostatic interactions play a major role for explaining the structure of the PNA CT band in water, the theoretical prediction of the observed red shift is improved by the explicit consideration of local hydrogen bonding of PNA to water. For isolated PNA, we predict that the dipole moment of the second excited state (S_2) is 9.6 D greater than ground state (S_0) dipole, which is in good agreement with experimental information (8.2−9.3 D). Calculation of charge transfer indexes for the two first excitations of PNA in water indicates that despite the feature that a small fraction of S_1 states (<5%) may exhibit some CT character, CT states in solution are mainly associated with $S_2 \leftarrow S_0$ transitions.

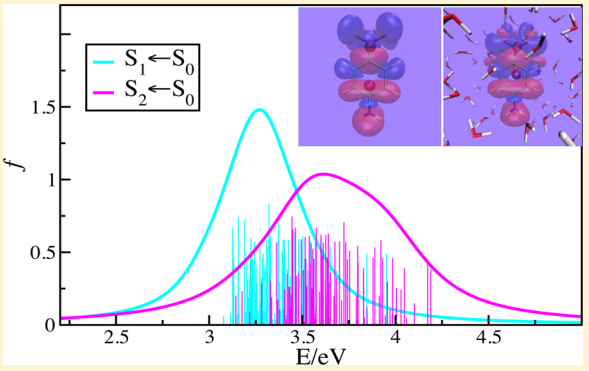

INTRODUCTION

The electronic properties of "push and pull" dyes is a subject of strong interest in chemistry, materials science, and biotechnology.[1] Push and pull dyes also exhibit large nonlinear optical properties with a wide range of applications in the design of photonic devices.[1−4] A specific class of push and pull dyes are disubstituted benzenes.[5] These dyes are characterized by the presence of electron donor and electron acceptor substituents connected by a π-system. Upon excitation, an intramolecular charge transfer (CT) process takes place leading to the formation of a CT absorption band. The structure of this band is strongly dependent on the interactions with the environment.[6] Analysis of the dependence of the CT process on the length of the π-system[5] as well as the characterization of the electronic density reorganization in terms of CT spatial indexes were reported.[7−10] Solvent effects on the electronic absorption spectra of different molecular species exhibiting CT states have been the subject of numerous works.[11−20]

The electronic properties of disubstituted benzenes and in particular of *p*-nitroaniline (PNA) where the substituents are the electron donor amine group ($-NH_2$) and the acceptor the nitro group ($-NO_2$), which are linked via a phenyl ring, have been widely investigated.[5,11,14−16,20−28] The dependence of the CT band shift on the nature of the solute−solvent interactions has been also investigated.[23,24] In general, solvent effects lead to a bathochromic shift of the CT band relative to the gas phase value. This shift is strongly dependent on the solvent polarity[23,24] and thermodynamic conditions.[28] Here, we will focus on a strong polar solvent (water), where the CT band shift is −0.98 eV.[14,29] The origin of the CT bathochromic shift in water was related to the energetic stabilization of the PNA ground state due to Coulombic interactions with the solvent.[23]

Recent theoretical investigations of PNA in different solvents have been reported.[23,24,26] Kosenkov and Slipchenko[24] used a quantum mechanics/effective fragment potential approach (QM/EFP), where the QM solute (PNA) is described by an ab initio method and the solvent molecules are represented by effective fragment potentials parametrized by first-principles calculations. A similar QM/EFP approach was adopted by Sok et al.[23] that reported a TDDFT/EFP1 study for the first excitation of PNA in water.[23] Thermal sampling with QM/EFP has been exploited by molecular dynamics simulations for the QM system coupled to the EFP solvent molecules.[23] Frutos-Puerto et al. presented a discussion on the preferential solvation effect on the solvatochromic shifts of PNA by using a quantum mechanics/molecular mechanics (QM/MM) approach, where

Received: February 22, 2016
Revised: May 17, 2016
Published: May 17, 2016

DOI: 10.1021/acs.jpca.6b01797
J. Phys. Chem. A 2016, 120, 3878−3887

different solvents are represented by classical force-fields.[26] More recently, Cardenuto et al.[28] investigated the electronic absorption spectrum of PNA in supercritical water by using a sequential QM/Monte Carlo (MC) methodology[30] in which the MC sampling relied on a classical force-field.

Although it is known that the CT band of PNA in water is mainly determined by Coulombic interactions,[23] some specific issues concerning the nature of CT states in water deserve further analysis. They include the relationship between the structural dynamics and the electronic properties of the dyes and the characterization of the CT states in solution. To investigate these issues, here we adopt a first-principles approach. Initially, a Born−Oppenheimer molecular dynamics (BOMD)[31] was carried out for a PNA−water solution and for isolated PNA at the same temperature of the solution. Then, sequentially, the electronic properties in water were determined by quantum mechanics calculations using a selected number of configurations generated by BOMD. Emphasis was placed on the analysis of the electronic absorption spectrum of PNA in water that was calculated by using time-dependent density functional theory (TDDFT).[32] Recent developments in density functional theory, specifically double hybrid density functionals,[33] made possible the application of TDDFT to the accurate calculation of excitation energies[34] even for systems involving charge transfer excitations. In these cases, it is well-known that widely used approximations for the exchange-correlation functional present serious limitations.[25] In this work, we also investigate the accuracy of a double hybrid functional (B2GP-PLYP)[33,35] for predicting the electronic properties of PNA in water.

Other fundamental issue deserving further attention concerns the nature of the excited states in solution that is strongly dependent on the solute−solvent interactions and consequently on the specific organization of the solvent around the solute species. In this sense, we explore, probably for the first time, the calculation of charge transfer indexes[8] for a dye in liquid water. The present calculation of CT indexes underlines the feature that only a fraction of electronic excitations of PNA in water can be characterized as CT.

This work is organized as follows. After presenting some details on the computational procedures, we investigate the structure and electronic properties of small PNA−water complexes. Then, we discuss results for the structure and the vibrational dynamics of isolated PNA and PNA in water. The structure was investigated through the calculation of the radial distribution functions (RDFs) with emphasis on solute−solvent hydrogen bond (HB) correlations. The calculation of the vibrational properties relies on the calculation of time correlation functions by using the Born−Oppenheimer dynamics. This is followed by the analysis of the electronic properties of PNA in water, including excited state dipole moments, and the electronic absorption spectrum. Finally, a discussion on CT indexes for PNA in water is presented and we conclude by stressing the importance of adopting a sequential TDDFT/BOMD approach for a better understanding of the electronic properties of push and pull dyes in solution as well as by the interest in calculating CT indexes in solution.

■ COMPUTATIONAL DETAILS

Gas Phase Calculations for PNA and PNA−Water Aggregates. Geometry optimizations for PNA and complexes of PNA with 5 and 10 water molecules were carried out with the BLYP-D3 functional, which is a combination of the Becke exchange functional[36] with the Lee, Yang, and Parr correlation functional[37] plus an empirical correction to the dispersion interactions D3.[38] The Dunning's cc-pVDZ (pvdz) basis-set[39] was used in the geometry optimizations. Excitation energies for PNA and PNA−water aggregates were calculated with TDDFT with the double hybrid B2GP-PLYP[33,35] with the Tamm-Dancoff approximation (TDA) to the TDDFT excitation energies.[40] Geometry optimizations and TDDFT excitation energies were carried out with the ORCA program[41] For the isolated PNA molecule, excitation energies and excited state dipole moments were also calculated by using the equation-of-motion second-order approximate coupled cluster singles and doubles method (EOM-CC2)[42,43] as implemented in the PSI4 program.[44] Excitation energies were calculated with the Dunning's aug-cc-pVDZ basis-set[39] (apvdz in a simplified notation).

Born−Oppenheimer Molecular Dynamics for PNA and PNA in Water. BOMD for PNA in water was carried out at a target temperature of T = 298 K for a system of one PNA molecule and 96 water molecules (N_w = 96) in a cubic box of size L = 14.59 Å with periodic boundary conditions. Additional BOMD was carried out, also at T = 298 K, for an isolated PNA molecule in a cubic box with the same size L. For the isolated PNA molecule, the Martyna and Tuckerman Poisson solver for nonperiodic boundary conditions[45] was employed. The BLYP combination of the Becke exchange functional[36] with the Lee, Yang, and Parr correlation functional[37] plus an empirical correction to the dispersion interactions D3[38] or BLYP-D3 was adopted for BOMD that was carried out with the hybrid Gaussian and plane-wave method (GPW)[46] as implemented in the CP2K program.[47] The choice of the BLYP-D3 model was driven by first-principles molecular dynamics of liquid water[48] indicating that this approach leads to a correct description of the water structure when comparison is made with experimental information. Goedecker, Teter, and Hutter (GTH) norm-conserving pseudopotentials[49] were used for representing the core electrons and only valence electrons were explicitly included in the quantum mechanical density functional theory (DFT) calculations of the forces to generate the dynamics. In the GPW approach, Kohn−Sham orbitals are expanded into atom-centered Gaussian-type orbital functions, whereas the electron density is represented with an auxiliary plane-wave basis-set. A double-ζ-valence-polarization (DZVP-MOLOPT-SR)[50] was used to represent the Gaussian orbitals and the charge density cutoff for the auxiliary basis-set was 280 Ry. The self-consistent-field energy threshold for calculating the electronic density was 10^{-6} Hartree. The time step was 0.5 fs and the total BOMD time was 50 ps (100 000 steps). For temperature control, we employed the canonical sampling velocity rescale thermostat (CSVR).[51] Average properties were calculated by using the last 25 ps of the BOMD run.

Excitation energies for PNA in water were calculated with TDDFT with the double hybrid B2GP-PLYP[33,35] with the Tamm-Dancoff approximation (TDA) to the TDDFT excitation energies.[40]

The electronic absorption spectra of PNA in water was calculated by using 100 selected configurations equally separated in time from the last 25 ps of dynamics. To calculate the electronic spectrum, we defined supermolecular structures with the solute (PNA) plus a given number (NQS) of explicit solvent molecules. This quantum system (QS) is embedded (EMB) in the polarizing electrostatic field of the remaining

DOI: 10.1021/acs.jpca.6b01797
J. Phys. Chem. A 2016, 120, 3878−3887

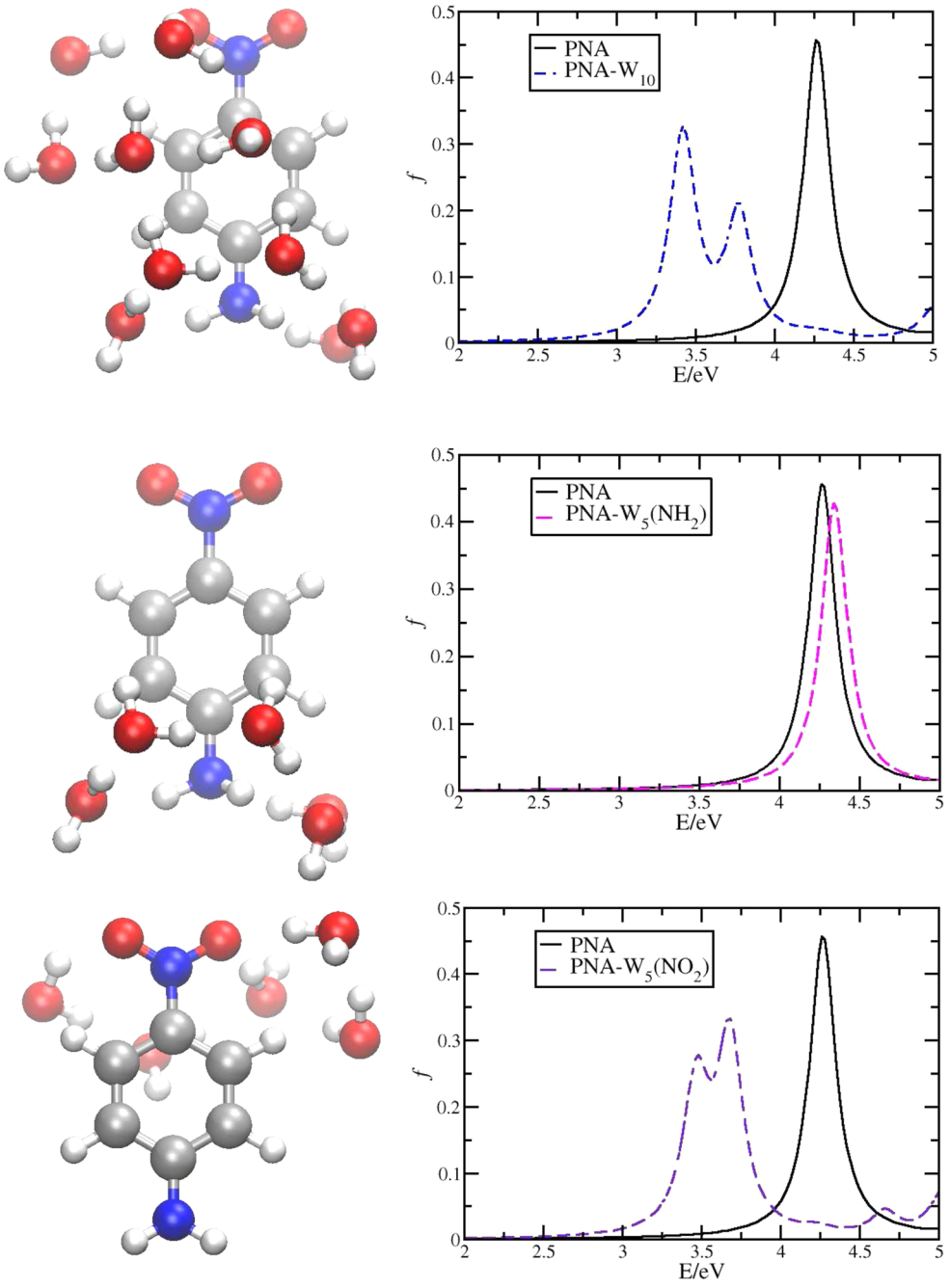

Figure 1. Left: BLYP-D3/pvdz optimized structures for complexes of PNA with n water molecules (PNA–W_n; n = 5, 10). Right: electronic absorption spectra for the isolated PNA (full lines) and PNA–W_n (dashed lines). Top panels, PNA–W_{10}; middle panels, PNA–W_5 complex, where the water molecules interact with the NH_2 group; bottom panels, PNA–W_5 complex, where the water molecules interact with the NO_2 group. The BLYP-D3 method was used for geometry optimizations. Time dependent density functional theory (TDDFT) excitation energies were calculated with the double hybrid B2GP-PLYP functional. The aug-cc-pVDZ basis set was used in the TDDFT calculations.

(N_w-NQS) solvent molecules, which were represented by atomic charges. The NQS solvent molecules explicitly included in the quantum system were selected by ordering the solvent molecules as a function of their distance to the nitrogen atoms of the PNA nitro and amine groups. Thus, for a given NQS value we selected NQS/2 water molecules closest to the nitro group (N atom) plus NQS/2 molecules closest to the amine group. This system is then embedded in the electrostatic field defined by the remaining (N_w-NQS) atomic point charges of the water molecules.

Results for NQS = 0 (EMB) correspond to the PNA molecule embedded in the charge distribution of the water molecules. The charges of the embedding water molecules were estimated by the polarizable continuum model (PCM) method,[52] where the environment is represented by a continuum medium with the experimental dielectric constant of water (ε = 78.35). The atomic charges were calculated by fitting to the electrostatic potential with the CHELPG[53] method. At the second-order Møller–Plesset perturbation theory (MP2)[54] level and by using the Dunning's aug-cc-pVDZ basis-set[39] (apvdz in a simplified notation), this approach leads

DOI: 10.1021/acs.jpca.6b01797
J. Phys. Chem. A 2016, 120, 3878–3887

Table 1. Excitation Energies (in eV) and Oscillator Strengths (in Parentheses) for the Gas Phase PNA and Optimized Structures of PNA−Water Complexes Shown in Figure 1[a]

		PNA	PNA−W_{10}	PNA−W_5(I)	PNA−W_5(II)
$S_0 \rightarrow S_1$	$n \rightarrow \pi^*$	3.77 *3.78*	3.42 (0.310)	3.73	3.47 (0.222)
$S_0 \rightarrow S_2$	$\pi \rightarrow \pi^*$	4.27 (0.46) *4.31 (0.42)* [4.24]	3.77 (0.189)	4.30	3.68 (0.291)
$S_0 \rightarrow S_3$	$n \rightarrow \pi^*$	4.39 *4.40*	4.21 (0.006)	4.34 (0.426)	4.21 (0.003)
$S_0 \rightarrow S_4$		4.64 (0.002) *4.60*	4.36 (0.006)	4.67	4.29 (0.002)
$S_0 \rightarrow S_5$		5.12 (0.001)	5.01 (0.009)	5.53 (0.030)	5.02 (0.061)
$S_0 \rightarrow S_6$	$\pi \rightarrow \pi^*$	5.48 (0.077) [5.48]	5.46 (0.008)	5.59 (0.030)	5.36 (0.001)

[a]Assignments are made for the transitions with experimentally known excitation energies and for the three lowest transitions. Geometries optimized at BLYP-D3/pvdz level. TDDFT excitations energies were calculated with the B2GP-PLYP exchange-correlation functional and the EOM-CC2 method (gas phase PNA, values in italic). Theoretical calculations carried out with the apvdz basis-set. Experimental values for gas phase PNA from Millefiori et al.[21] are shown in brackets.

to $q_O = -0.786$ au and $q_H = 0.393$ au. In keeping with a recent work on liquid and $scCO_2$[55] we have verified that the electronic absorption spectrum of PNA in water is not significantly dependent on the choice of the electrostatic embedding and quite similar results are predicted by using charges from different classical force field models. Excitation energies of PNA in liquid water were calculated with the apvdz basis-set. The excitation spectra were constructed by fitting a Lorentzian distribution of 0.10 eV width to the excitation energies and oscillator strengths.

The electronic densities and dipole moments for the ground and excited states of gas phase PNA and for the selected configurations of PNA in water were calculated with the Gaussian-09 program.[56] These calculations were carried out with the CAM-B3LYP[57] and B2GP-LYP[33,35] functionals. The excited state electronic densities calculated with B2GP-PLYP are not accounting for the "CIS(D)" like part correction to the B2GP-LYP excitation energies. Therefore, they correspond to the electronic densities predicted by the B2GP-LYP functional.[33,35] The TDA[40] was adopted. Charge transfer indexes[8,58] were calculated with a program coded by Jacquemin.[59]

RESULTS AND DISCUSSION

Electronic Absorption Spectra of Gas Phase PNA and PNA−Water Complexes. Figure 1 shows the structure of PNA−water complexes. To investigate the influence of the local hydrogen bond (HB) of PNA with water molecules, and to assess separately the influence of HB to the PNA amine and nitro groups on the electronic absorption spectra the structure of three PNA−water complexes was determined by carrying out geometry optimizations at the BLYP-D3/pvdz theoretical level. By carrying out geometry optimizations for a PNA−water complex, we have verified that hydrogen bond lengths calculated at the BLYP-D3 level are in good agreement with MP2[54] results. Therefore, it is expected that this theoretical level is adequate to investigate the structure of the larger PNA−water aggregates. The optimized structures correspond to local minima on a complex energy surface and were determined with the specific purpose of investigating the influence of local HB on the electronic absorption spectra. Two complexes of PNA with five water molecules were optimized. The first one (left bottom panel of Figure 1) illustrates HB formation in the PNA−W_5 complex through interactions with the PNA nitro group. The second (left middle panel of Figure 1) illustrates HB formation through the amine group. The structure of a PNA−water complex with 10 water molecules is illustrated in the left top panel of Figure 1. The electronic absorption spectra for the different complexes are also shown in Figure 1 (right panels), where the intensity f is the oscillator strength. Our results show that in comparison with the isolated PNA molecule, HB formation with the PNA nitro and amine groups influence in a different way the electronic energy absorption by PNA−water complexes. The electronic absorption spectrum of the complex involving HB to the amine group is not significantly modified in comparison with the spectrum of the isolated species and only a small blue shift is observed (middle panel of Figure 1). The weak dependence of the electronic absorption on hydrogen bonding interactions with the amine group was pointed out by different works.[60,61] On the other hand, HB to the nitro group leads to a significant red shift of the first electronic absorption band relative to the isolated species. As shown in the right top and bottom panels of Figure 1, the first electronic absorption bands in the PNA−W_{10} and PNA−W_5 for HB to the nitro group are quite similar although some differences in the intensities are observed. For gas phase PNA, comparison between the theoretical results (B2GP-PLYP[33,35] and EOM-CC2[42,43]) shown in Table 1 and the experimental excitation energies[21] shows a very good agreement, leading credence to the presently adopted model (B2GP-PLYP/apvdz) to investigate the electronic properties of PNA in water. The magnitude of the red shift, relative to the isolated PNA species of the first absorption band in the PNA−W_{10} complex (∼−0.85 eV) is close to the experimentally observed value (−0.98 eV)[14,29] and reflects the importance of the role played by hydrogen bonding to the nitro group on the red shift of the PNA CT band in liquid water. However, it is expected that the results for the optimized structures overestimate the shift due to the absence of thermal effects. These effects need a statistical sampling procedure to be taken into account.

Structure and Vibrational Properties of PNA in Liquid Water. *Structure.* Structural information on the PNA−water solution can be assessed by calculating the radial distribution functions (RDFs), specifically those related to specific interactions between the nitro and amino groups with water. The RDFs describing these interactions are shown in Figure 2. Additional data on the structure and coordination numbers are reported in Table 2. Comparison between the structural correlations with water of the nitro and amine groups, particularly, between the role played by the PNA as hydrogen bond acceptor described by $O[NO_2]...H_w$ correlations, and hydrogen bond donor, described by $H[NH_2]...O_w$ correlations, indicates that PNA in water is a better H acceptor than donor. Specifically, as shown in Table 2, the average coordination numbers $N_c(r_{min})$ are 1.4 and 1.1 for $O[NO_2]...H_w$ and $H[NH_2]...O_w$, respectively. Further information on the organization of the water molecules around the nitro and

DOI: 10.1021/acs.jpca.6b01797
J. Phys. Chem. A 2016, 120, 3878−3887

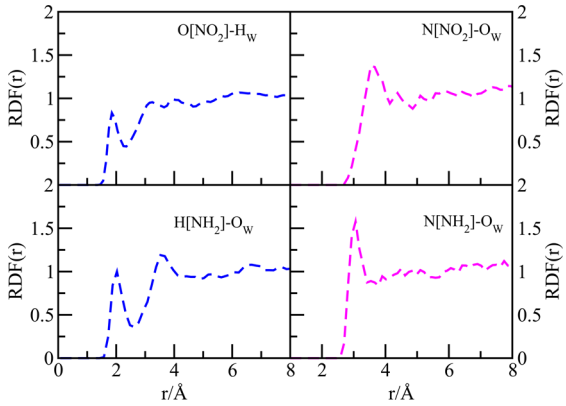

Figure 2. Radial distribution functions (RDFs). Left panels: RDFs describing PNA−water hydrogen bonding, where PNA plays the role of proton acceptor (top left) and proton donor (bottom left). Right panels: RDFs related to the N−O_w correlations involving the nitrogen atom of the NO_2 (top right) and NH_2 (bottom right) groups with the water oxygen atoms (O_w).

Table 2. Data on the Structure of the PNA−Water Solution[a]

	r_{max}	$N_c(r_{max})$	r_{min}	$N_c(r_{min})$
$O(NO_2)-H_W$	1.9	0.5	2.3	1.4
$H(NH_2)-O_W$	2.0	0.5	2.6	1.1
$N(NO_2)-O_W$	3.6	2.5	4.9	12.1
$N(NH_2)-O_W$	3.1	2.2	3.7	4.3
$N(NH_2)-H_W$	2.0	0.2	2.4	0.4
$O(NO_2)-O_W$	3.1	1.9	4.2	8.2
O_W-O_W	2.8	1.8	3.5	5.2

[a]Average values (in Å) for the maxima (r_{max}) and minima (r_{min}) positions of the radial distribution functions (RDFs) and corresponding coordination numbers N_c.

amine groups is given by the RDFs describing the N[NO_2]−O_w and N[NH_2]−O_w structural correlations. Integration of these RDFs up to the first minima leads to coordination numbers of 12.1 and 4.3, which represent the average number of water molecules in the first coordination shell of the nitro and amine groups, respectively. Data on the RDF related to the oxygen atom of PNA and water oxygen atoms correlations (O[NO_2]−O_W) as well on the RDF describing the water oxygen−oxygen atoms correlations [O_W−O_W] are reported in Table 2. Integration of these RDFs up to the first maximum leads to an estimate of the average number of water molecules in close interaction with the PNA oxygen atom (1.9) and the number of water molecules in close interaction with a reference water molecule in liquid water (1.8). This result indicates that the interactions between the oxygen atoms of liquid water and between the water and PNA oxygen atoms are similar.

Figure 3 (left panels) shows the distributions P[d(N—O)] and P[d(N—H)] of the bond lengths d(N—O) and d(N—H) for the gas phase PNA and for PNA in water. The results indicate that due to hydrogen bonding, in liquid water the d(N—O) bond length is slightly increased relative to its gas phase value. The average values of d(N—O) are 1.262 and 1.284 Å for gas phase PNA and PNA in water, respectively. Quite similar values for the average d(N—H) bond lengths are presently predicted for the PNA molecule in the gas phase and water (1.017 and 1.025 Å, respectively). The average θ(O—N—O) angle for isolated PNA is 123.9°, and the value for PNA in water is 120.5°. However, the average d(O—O) distances

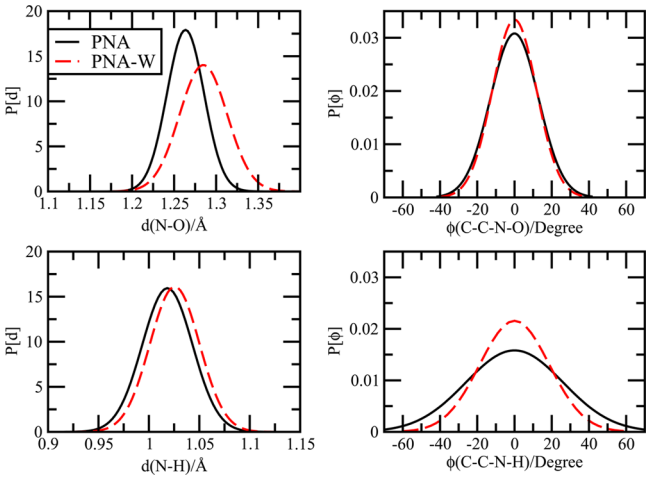

Figure 3. Distribution of structural parameters from BOMD of PNA in the gas phase and liquid water (PNA−W). Left panels: distributions P[d] of the d(N—O) and d(N—H) bond distances. Right panels: distribution P[ϕ] of the dihedral angle ϕ describing the twisting of the NO_2 [ϕ(C—C—N—O)] and NH_2 [ϕ(C—C—N—O)] groups around the ring plane.

for PNA and PNA in water are identical (2.23 Å), a feature that can be explained by the increase of the d(N—O) distance in water relative to the isolated species. This structural change contributes to increase the dipole moment of PNA in water. The right panels of Figure 3 show the distribution of the dihedral angles ϕ(C—C—N—O) (top panel) and ϕ(C—C—N—H) (bottom panel) for PNA and PNA in water and when ϕ = 0 the plane defined by nitro or amine groups coincides with the ring plane. This parameter provides information on the twisting dynamics of the nitro and amine groups. For both the nitro and amine groups, the distributions P[ϕ] indicate significant deviations from the equilibrium value (ϕ = 0). P[ϕ(C—C—N—O)] shows an expected Gaussian behavior with a maximum value at ϕ = 0. Quite similar distributions of ϕ(C—C—N—O) are observed for PNA and PNA in water. Comparison between P[ϕ(C—C—N—H)] for PNA and PNA in water indicates that the NH_2 twisting dynamics is modified by the interactions with the water molecules. These interactions lead to a slightly narrower P[ϕ(C−C−N-H)] in water.

As previously discussed, significant deviations from ϕ(C—C—N—O) = 0 are observed for PNA in water. The adequate treatment of the nitro and amine twisting dynamics is important for predicting the electronic properties of PNA. It has been verified that the twisting of the nitro group relative to the conjugated structure leads to a broadening of the electronic absorption spectrum and stabilizes the charge transfer excited state.[29]

Vibrational Spectrum. As in previous BOMD studies,[55] the vibrational spectrum is presently investigated through the calculation of time correlation functions. For example, the distribution of the ν(N—X) (X = O,H) stretching frequency of PNA can be analyzed by calculating the Fourier transform of the average velocity autocorrelation function defined as $C_{AA}(t)$ = $\langle \delta A(t + t_i)\ \delta A(t_i)/\delta A(t_i)\ \delta A(t_i) \rangle$ where $A = \frac{dy}{dt}$, t_i is a time origin, y = d(N—X), and $\delta A \equiv A - \langle A \rangle$. Figure 4 shows the distribution of the N—O [ν(N—O)], top panel) and N—H [ν(N—H)], bottom panel) frequencies.

The ν(N—O) stretching frequency distribution of gas phase PNA at T = 298 K indicates the presence of a doublet at

DOI: 10.1021/acs.jpca.6b01797
J. Phys. Chem. A 2016, 120, 3878−3887

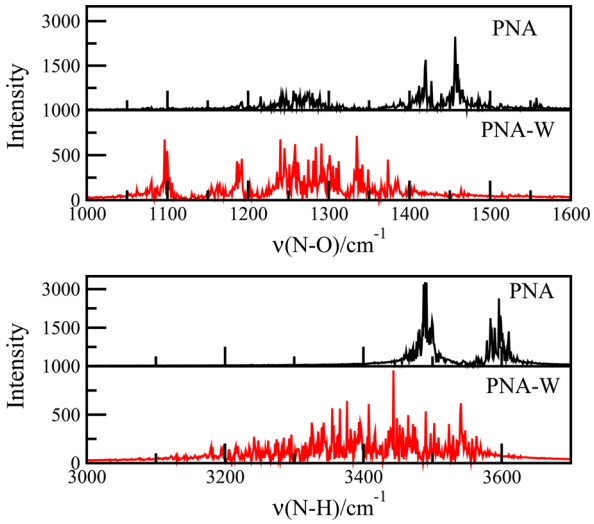

Figure 4. Frequency distributions describing the N—O (top) and N—H (bottom) stretching dynamics of isolated PNA (black) and PNA in water (red).

~1460/1420 cm^{-1} corresponding to the asymmetric N—O_2 stretching. At lower frequencies, a maximum at ~1282 cm^{-1} associated with the symmetric stretching can also be identified.

Upon hydration, a much broader ν(N—O) distribution is observed. Two maxima near 1300 and 1330 cm^{-1} are present although a clear assignment is difficult due to the broad nature of the calculated distribution. Despite this limitation, experimental data for PNA in water also predicts a broad distribution in the 1300−1350 cm^{-1} range.[62,63] It is also known that the ν(N—O) distribution exhibits a strong dependency on the solvent and thermodynamic conditions.[62,63] Our results show a ~ 160 cm^{-1} red shift of the whole ν(N—O) distribution of PNA in liquid water relative to the gas phase result, which is a fingerprint of hydrogen bonding of the PNA nitro group to the water molecules.

The ν(N—H) stretching frequency distribution of gas phase PNA shows two maxima at 3596 and 3492 cm^{-1}. These maxima correspond to the asymmetric [ν_{as}(N—H)] and symmetric [ν_{sym}(N—H)] N—H stretching modes. Experimental data is available for solid PNA[64] and for PNA in ethanol and methanol.[63] For solid PNA, two maxima at 3482 cm^{-1} [ν_{as}(N—H)] and 3361 cm^{-1} were reported.[64] For PNA on ethanol, a broad distribution with a single maximum at ~3400 cm^{-1} was predicted.[63] We are not aware of Raman experiments for gas phase PNA. As expected, our results for isolated PNA are blue-shifted relative to the experimental values for ν(N—H) in condensed phase. However, our predictions for gas phase PNA are in very good agreement with the scaled DFT frequencies reported by Kavitha et al.: ν_{as}(N—H) = 3590 cm^{-1} and ν_{sym}(N—H) = 3478 cm^{-1}.[64] Our result for PNA in water shows a broad distribution that peaks nearly at ν(N—H)= 3440 cm^{-1}, which is in good agreement with Fujisawa et al. (~3400 cm^{-1}).[63] Comparison between the maximum position of the ν(N—H) distribution in water (3440 cm^{-1}) and the gas phase value for [ν_{as}(N—H)] (3596 cm^{-1}) indicates that ν(N—H) is red-shifted by ~160 cm^{-1} upon hydration.

Electronic Absorption of PNA in Water. Table 3 presents data for the dipole moments of the ground and excited states of isolated PNA and PNA in water. Oscillator strengths for the three lowest excited states are also reported. The presently predicted ground state dipole moment of gas phase PNA (5.2 D) is in good agreement with the experimental data of 5.5 D from Sinha et al.[65] although it is 1 D below a second prediction from the same group (6.2 D).[66] However, it should be noticed that the experimental data reported in Table 3 is for PNA in a dioxane solution at T = 298 K.[65,66] A better agreement with the higher experimental value (6.2 D)[66] is observed for the CC2 (6.4 D) and CAM-B3LYP (7.1 D) results.

Excited state dipole moments were calculated in the ground-state geometry and are compared with experimental information relying on electro-optical absorption methods that are adequate to investigate intramolecular CT in vertical excited states.[65] The B2GP-LYP dipole moment for the S_2 excited state of gas phase PNA (14.8 D) is also in reasonable agreement with experimental information.[65,66] Moreover, the present DFT results for the dipole moment change upon the $S_2 \leftarrow S_0$ transition [9.6 D (B2GP-LYP); 9.8 D (CAM-B3LYP)] are also in good agreement with experimental information for PNA in a dioxane solution (8.5 ± 0.5;[65] 9.3 D[67]). Comparison between DFT and EOM-CC2 results for PNA (italic values in Table 3) shows a very good agreement. The B2GP-PLYP result for the ground state dipole moment of PNA in water is 11.1 ± 0.3 D, which is 6 D above the gas phase dipole. A smaller change of the PNA ground state dipole moment upon hydration (2.8 D) is predicted at the CAM-B3LYP level. The average value of the S_1 state dipole moment is modified upon hydration. The changes are 8.1 ± 0.5 D (B2GP-LYP) and 5.7 ± 0.4 D (CAM-B3LYP). The average oscillator strengths $\langle f \rangle$ for the $S_1 \leftarrow S_0$ transition are 0.21 ± 0.0 (B2GP-PLYP) and 0.10 ± 0.01

Table 3. Dipole Moments (μ in D) and Oscillator Strengths (f) of PNA and PNA in Water (PNA−W)[a]

	PNA		PNA−W	
	μ	f	$\langle\mu\rangle$	$\langle f\rangle$
S_0	5.2 [5.5 ± 0.2][65][6.2][66]		11.1 ± 0.3	
	(7.1) *6.4*		(9.9 ± 0.3)	
S_1	4.4		12.1 ± 0.5	0.21 ± 0.02
	(4.0) *3.9*		(9.7 ± 0.4)	(0.10 ± 0.01)
S_2	14.8 [13.7 ± 0.5][65]	0.46 *0.43* [0.32][21]	13.7 ± 0.3	0.28 ± 0.02
	(16.9) *16.6*	(0.49)	(17.2 ± 0.3)	(0.35 ± 0.02)
S_3	4.9		11.5 ± 0.3	0.01
	(4.4) *4.1*		(10.6 ± 0.4)	(0.01)

[a]EOM-CC2 results for gas phase PNA in italics. CAM-B3LYP results in parentheses. Experimental data in brackets. Data for the ground (S_0) and the three lowest excited states (S_1, S_2, S_3). Theoretical calculations carried out with the apvdz basis-set. For PNA−W the NQS = 0 approximation was adopted.

DOI: 10.1021/acs.jpca.6b01797
J. Phys. Chem. A 2016, 120, 3878−3887

(CAM-B3LYP) thus indicating that this transition, which is forbidden in the isolated molecule, is enhanced in liquid water. The S_2 dipole moment is not significantly changed upon hydration and DFT calculations predict that the changes are below 1 D. The results also point out an increase of the S_3 dipole in water. However, in this case, the average f is close to zero.

The electronic absorption spectrum of PNA in water is shown in Figure 5. The specific role played by the electrostatic

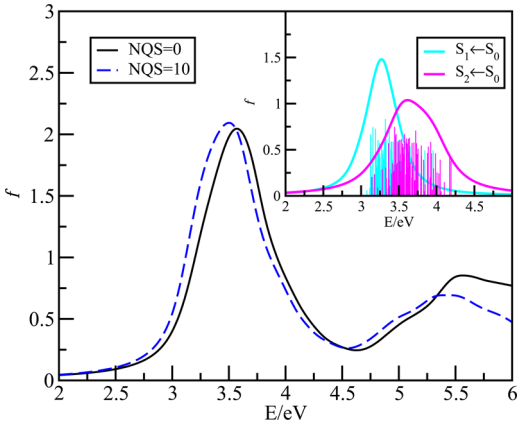

Figure 5. Electronic absorption spectrum of PNA in water. NQS is the number of water molecules explicitly included in the quantum system. For NQS = 0 only the electrostatic embedding of the water molecules is being taken into account. NQS = 10 means that the nearest 10 water molecules were included in the calculations (the 5 closest to NO_2 plus the five closest to NH_2). The inset panel shows the distributions of the $S_1 \leftarrow S_0$ and $S_2 \leftarrow S_0$ excitation energies for NQS = 10 and the vertical lines represent oscillator strengths.

background on the spectrum can be assessed by carrying out calculations with NQS = 0. As illustrated in Figure 5, electrostatic interactions play a significant role, leading to the appearance of a band with a maximum at 3.6 eV, which means a 0.7 eV red shift relative to the gas phase species (4.3 eV). The NQS = 10 curve corresponds to the average spectrum for a system including PNA plus 10 water molecules embedded in the electrostatic environment of the remaining water molecules ($N_w - 10$). This calculation allows us to assess the importance of taking explicitly into account local hydrogen bonding of PNA to water. The NQS = 10 curve shows a maximum at 3.5 eV. Therefore, the maximum of the first absorption band of PNA in water is red-shifted by ∼0.8 eV relative to the S_2 band of gas phase PNA. This result is in reasonable agreement with the experimental results, which are close to 1.0 eV.[14,29] The inset panel of Figure 5 shows for NQS = 10, the distributions of the first and second excitation energies that define the first absorption band of PNA in water. The distribution of the $S_1 \leftarrow S_0$ excitation energies shows a maximum at ∼3.2 eV that practically coincides with the experimental value,[14,29] whereas the distribution corresponding to $S_2 \leftarrow S_0$ excitation energies peaks at ∼3.6 eV.

Further analysis on the modifications of the electronic structure of PNA in water can be carried out through the introduction of qualitative charge transfer indexes associated with the charge reorganization upon excitation.[8] Details on the definition of CT indexes can be found in several recent works.[7−10] Here we will focus on the charge transfer (CT) excitation length, which is defined as $D_{CT} = |R_+ - R_-|$,[8] where R_+ and R_- are the barycenters of positive and negative electronic density, $\rho_+(r)$ and $\rho_-(r)$, respectively. In addition, the difference between the ground- and excited-state dipole moments can be estimated as $\|\mu_{CT}\| = D_{CT}\int\rho_+(r)dr = -D_{CT}\int\rho_-(r)dr = D_{CT}q_{CT}$, where q_{CT} is the transferred charge.[8]

Electronic density difference isosurfaces for PNA and two BOMD configurations of PNA in water are shown in Figure 6, where the charge barycenters are represented by spheres. Some CT indexes are reported in Table 4, where for completeness oscillator strengths are also reported. In general, a good agreement between B2GP-LYP and CAM-B3LYP results is observed. The following discussion relies on CAM-B3LYP results. Comparison between the two sets of data will be made only when it is justified. For isolated PNA, CAM-B3LYP calculations lead to D_{CT} = 3.1 Å, and q_{CT} = 0.74 au. Therefore, $\|\mu_{CT}\|$ = 9.9 D. For PNA in water, it is expected that the excitation process is strongly influenced by the solute−solvent interactions that include local hydrogen bonding as well as long-range polarization effects. Therefore, the electronic density

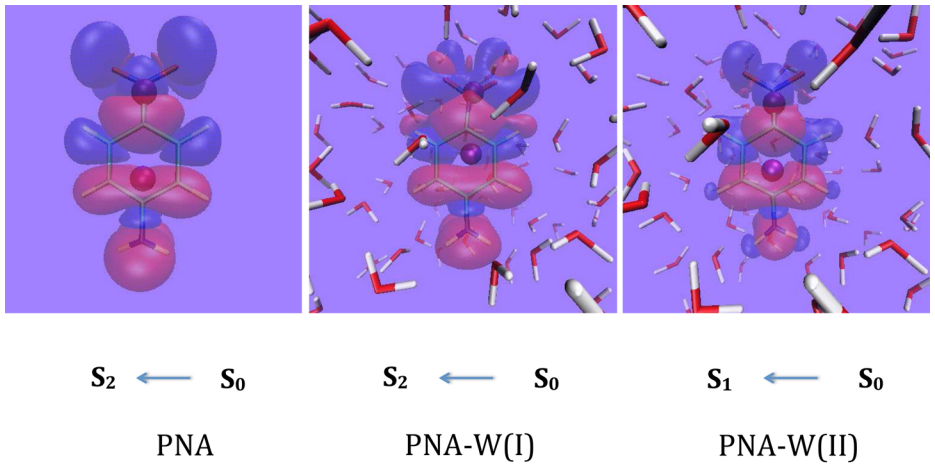

Figure 6. Electronic density difference $\Delta\rho(r) = \rho_{exc}(r) - \rho_{GS}(r)$ for PNA and PNA in water. The isocontour value is 0.0004 au and positive and negative density differences are represented as blue and red, respectively. The barycenters of the positive and negative $\Delta\rho(r)$ are indicated by the spheres (in purple). For PNA in water, two BOMD configurations I and II are illustrated and the isosurfaces correspond to the transitions $S_0 \leftarrow S_2$ (I); and $S_0 \leftarrow S_1$ (II).

DOI: 10.1021/acs.jpca.6b01797
J. Phys. Chem. A 2016, 120, 3878−3887

Table 4. Charge Transfer Indexes for PNA and PNA in Water[a]

	f	D_{CT}	q_{CT}	$\|\mu_{CT}\|$
PNA				
$S_2 \leftarrow S_0$	0.46 (0.38)	2.10 (3.11)	0.96 (0.67)	9.6 (9.9)
PNA–W(I)				
$S_2 \leftarrow S_0$	0.53 (0.49)	2.20 (2.60)	0.96 (0.92)	10.1 (11.5)
PNA–W(II)				
$S_1 \leftarrow S_0$	0.57(0.51)	2.20 (2.67)	0.39 (0.46)	4.0 (5.9)
PNA–W				
	$\langle f \rangle$	$\langle D_{CT} \rangle$	$\langle q_{CT} \rangle$	$\langle \|\mu_{CT}\| \rangle$
$S_2 \leftarrow S_0$	0.43 ± 0.01	2.1 ± 0.1	0.82 ± 0.02	8.2 ± 0.3
	(0.42 ± 0.01)	(2.5 ± 0.1)	(0.83 ± 0.01)	(9.8 ± 0.2)

[a] D_{CT} in Å. q_{CT} in au. $\|\mu_{CT}\|$ in D. PNA–W(I) and PNA–W(II) are two configurations from BOMD. The average values are for PNA in water (PNA–W). CAM-B3LYP results in parentheses.

reorganization is very dependent on the specific configuration generated by the BOMD sampling procedure. This is illustrated by the middle and right panels of Figure 6 for two configurations. Configuration I (middle panel of Figure 6) has an oscillator strength $f = 0.5$ ($S_2 \leftarrow S_0$) and $f = 0$ for the first excitation. For configuration II (right panel) $f = 0.49$ ($S_1 \leftarrow S_0$), whereas for the second excitation, $f = 0$. For configuration I, the dipole moment is significantly changed upon the $S_2 \leftarrow S_0$ transition ($\|\mu_{CT}\| = 11.5$ D. For configuration II, $\|\mu_{CT}\| = 5.9$ D ($S_1 \leftarrow S_0$). It should be noticed that B2GP-LYP leads to smaller values of D_{CT}, when comparison is made with CAM-B3LYP.

Although, the $S_1 \leftarrow S_0$ transition becomes allowed in liquid water, the average value of its oscillator strength is still smaller than the average oscillator strength ($\langle f \rangle$) of the $S_2 \leftarrow S_0$ transition. What is more important, the average charge transferred upon excitation, q_{CT}, for $S_1 \leftarrow S_0$ (0.34 ± 0.01 au) is smaller than that one for $S_2 \leftarrow S_0$ (0.76 ± 0.02). In addition, for the first excitation $\langle D_{CT} \rangle = 1.2 \pm 0.1$, which is much smaller than $\langle D_{CT} \rangle$ for the S_2 state (2.5 ± 0.1 Å at the CAM-B3LYP level). Therefore, the present results indicate that there is no charge transfer/charge separation for the $S_1 \leftarrow S_0$ transition in liquid water, despite the feature that for a small fraction of configurations (<5%) this transition may exhibit some CT character. On the other hand, not all the $S_2 \leftarrow S_0$ transitions of PNA in liquid water lead to charge transfer. For nearly 20% (CAM-B3LYP) and 40% (B2GP-PLYP) of the selected configurations, the oscillator strength f is below 0.3 and $q_{CT} < 0.4$ au. It seems reasonable to assumed that $S_2 \leftarrow S_0$ can be identified as a CT transition when $f > 0.3$ and $q_{CT} > 0.5$ au. By adopting this criterium (driven by the values of f and q_{CT} in the gas phase PNA), we estimate that ~60–75% of the $S_2 \leftarrow S_0$ excitations of PNA in water will be related to a CT process. Within the adopted criterium, the average values of CT indexes for PNA in water are reported in Table 4. It is interesting to notice that quite similar values of $\|\mu_{CT}\|$ are predicted for isolated and hydrated PNA (9.9 D). If the criterium for CT is relaxed, we predict that $\langle \|\mu_{CT}\| \rangle = \langle D_{CT} \rangle \langle q_{CT} \rangle = 8.1 \pm 0.4$ D, However, this value should not be interpreted as an estimate only associated with $S_2 \leftarrow S_0$ CT excitations in water.

CONCLUSIONS

Born–Oppenheimer molecular dynamics for a PNA–water solution was carried out with the BLYP-D3 functional. The choice of this functional was driven by a recent BOMD of liquid water[48] that pointed out a very good agreement between the structure predicted by BLYP-D3 and experimental data. Radial distribution functions, vibrational frequencies, and electronic properties of the solution were investigated. The present results provide a set of useful information for a better understanding on the relationship between the structure, hydrogen bonding, vibrational dynamics, and the electronic properties of the PNA–water system. Moreover, we have also discussed a fundamental question concerning the hydration of PNA in water, namely, the nature of the excited states in solution. This discussion relies on the calculation of charge transfer indexes describing the electronic density reorganization upon excitation.[7−10] The electronic properties of PNA in water were investigated by carrying out DFT calculations for a selected set of configurations generated by Born–Oppenheimer molecular dynamics. Emphasis was placed on the electronic absorption spectrum of PNA in water that was calculated by using TDDFT with the B2GP-PLYP double hybrid functional. Our results show that for the isolated PNA molecule, B2GP-PLYP excitation energies are in very good agreement with those predicted by EOM-CC2 calculations and experiment.[21] This agreement supports the present choice of this functional for investigating the electronic properties of PNA in water.

A preliminary analysis of the electronic properties of small PNA–water aggregates allowed us to conclude that hydrogen bond interactions between the water molecules and the PNA nitro group red shift the maximum position of the absorption spectrum by ~0.85 eV relative to the gas phase PNA, whereas a small blue shift is induced by interactions with the amine group.

In line with the results for the small PNA–water aggregates, the structure of the PNA–water solution is characterized by hydrogen bonding interactions between the PNA nitro and amine groups and the water molecules. These interactions lead to structural changes with a fingerprint in the vibrational properties of PNA in water. Specifically, the ν(N—O) and ν(N—H) stretching frequencies in water are red-shifted by ~160 cm^{-1} relative to the gas phase species. We notice that our analysis on the vibrational fingerprint of hydrogen bonding is based on BOMD for PNA in water and a separated BOMD for isolated PNA at the same temperature.

For isolated PNA, the S_2 dipole moment is 9.6 D greater than the S_0 dipole, a result in good agreement with experimental information for PNA in a dioxane solution (8.5 ± 0.5;[65] 9.3 D).[14] The results indicate that the ground state dipole of PNA in water is increased relative to the gas phase species although different values are predicted by the B2GP-PLYP and CAM-B3LYP functionals. However, similar values of the S_2 dipole moment in the gas phase and water were obtained. The dipole moment and oscillator strength of the S_1 stated of PNA in water is considerably changed relative to isolated PNA. The average oscillator strength is in the 0.1–0.2 range thus providing an indication that $S_1 \leftarrow S_0$ transitions become allowed in solution. However, an analysis relying on the calculation of CT indexes strongly indicates that the PNA $S_1 \leftarrow S_0$ transition in liquid water is not a CT transition. In addition, it appears that not all the $S_2 \leftarrow S_0$ transitions of PNA in water are of CT nature. Our prediction for the peak position of the S_1 CT band of PNA in water (3.5 eV) is in good agreement with experimental data (~3.3 eV).[14,29] What is more important, we are providing evidence that although electrostatic interactions play a major role for explaining the structure of the S_1 CT band in water, the explicit consideration of PNA–water hydrogen bond improves the agreement between theoretical and

DOI: 10.1021/acs.jpca.6b01797
J. Phys. Chem. A 2016, 120, 3878–3887

experimental results. As illustrated in Figure 5, this conclusion relies on TDDFT calculations for 100 configurations from BOMD including a quantum system (QS) with the solute (PNA) plus a given number (NQS = 10) of explicit water molecules. This QS is embedded in the electrostatic field of the remaining N_w-NQS water molecules represented by point charges. The importance of taking into account the dynamics and its relationship with the electronic properties of PNA in water is well illustrated by the present results. The interest in the definition and calculation of topological indexes to investigate CT transitions in complex molecular systems should be stressed.

AUTHOR INFORMATION

Corresponding Author

*E-mail: bjcabral@fc.ul.pt. Phone: +351967844674.

Notes

The authors declare no competing financial interest.

ACKNOWLEDGMENTS

Work partially supported by CNPq, CAPES, FAPESP, INCT-FCx and BioMol (Brazil).

REFERENCES

(1) Imahori, H.; Umeyama, T.; Ito, S. Large π -Aromatic Molecules as Potential Sensitizers for Highly Efficient Dye-Sensitized. *Acc. Chem. Res.* **2009**, *42*, 1809−1818.

(2) Daniel, C.; Dupuis, M. Nonlinear Optical Properties of Organic Solids - Ab Initio Polarizabilities and Hyperpolarizabilities of Nitroanilines Derivatives. *Chem. Phys. Lett.* **1990**, *171*, 209−216.

(3) Jensen, L.; Van Duijnen, P. The First Hyperpolarizability of p-Nitroaniline in 1,4-Dioxane: A Quantum Mechanical/Molecular Mechanics Study. *J. Chem. Phys.* **2005**, *123*, 074307.

(4) Garza, A. J.; Scuseria, G. E.; Khan, S. B.; Asiri, A. M. Assessment of Long-Range Corrected Functionals for the Prediction of Non-Linear Optical Properties of Organic Materials. *Chem. Phys. Lett.* **2013**, *575*, 122−125.

(5) Berry, R. W. H.; Brocklehurst, P.; Burawoy, A. Electronic Spectra of Organic Molecules and Their Interpretation-VII. *Tetrahedron* **1960**, *10*, 109.

(6) Farztdinov, V. M.; Schanz, R.; Kovalenko, S. A.; Ernsting, N. P. Relaxation of Optically Excited p-Nitroaniline: Semiempirical Quantum-Chemical Calculations Compared to Femtosecond Experimental Results. *J. Phys. Chem. A* **2000**, *104*, 11486−11496.

(7) Le Bahers, T.; Pauporté, T.; Scalmani, G.; Adamo, C.; Ciofini, I. A TD-DFT Investigation of Ground and Excited State Properties in Indoline Dyes Used for Dye-Sensitized Solar Cells. *Phys. Chem. Chem. Phys.* **2009**, *11*, 11276−11284.

(8) Le Bahers, T.; Adamo, C.; Ciofini, I. A Qualitative Index of Spatial Extent in Charge-Transfer Excitations. *J. Chem. Theory Comput.* **2011**, *7*, 2498−2506.

(9) Ciofini, I.; Le Bahers, T.; Adamo, C.; Odobel, F.; Jacquemin, D. Through-Space Charge Transfer in Rod-Like Molecules: Lessons from Theory. *J. Phys. Chem. C* **2012**, *116*, 11946−11955.

(10) Adamo, C.; Le Bahers, T.; Savarese, M.; Wilbraham, L.; Garcia, G.; Fukuda, R.; Ehara, M.; Rega, N.; Ciofini, I. Exploring Excited States Using Time Dependent Density Functional Theory and Density-Based Indexes. *Coord. Chem. Rev.* **2015**, *304*−*305*, 166−178.

(11) Ledger, M. B.; Suppan, P. Spectroscopic Studies of Electron Distribution. *Spectrochim. Acta, Part A* **1967**, *23*, 641−653.

(12) Stahelin, M.; Burland, D. M.; Rice, J. E. Solvent Dependence of the Second Order Hyperpolarizability in p-Nitroaniline. *Chem. Phys. Lett.* **1992**, *191*, 245−250.

(13) Mikkelsen, K. V.; Kmit, M. Laser Field-Induced Charge-Transfer - Para-Nitroaniline Coupled to a Quantum Radiation-Field. *Theor. Chim. Acta* **1995**, *90*, 307−322.

(14) Thomsen, C. L.; Thøgersen, J.; Keiding, S. R. Ultrafast Charge-Transfer Dynamics: Studies of p-Nitroaniline in Water and Dioxane. *J. Phys. Chem. A* **1998**, *102*, 1062−1067.

(15) Moran, A. M.; Kelley, A. M. Solvent Effects on Ground and Excited Electronic State Structures of p-Nitroaniline. *J. Chem. Phys.* **2001**, *115*, 912.

(16) Moran, A. M.; Blanchard-Desce, M.; Kelley, A. M. Aromatic Versus Polyenic Linkers in Push-Pull Chromophores: Electron-Phonon Coupling Effects. *Chem. Phys. Lett.* **2002**, *358*, 320−327.

(17) Nugent, S.; Ladanyi, B. M. The Effects of Solute-Solvent Electrostatic Interactions on Solvatochromic Shifts in Supercritical CO_2. *J. Chem. Phys.* **2004**, *120*, 874−84.

(18) Ladanyi, B. M.; Nugent, S. The Effects of Solute-Solvent Electrostatic Interactions on Solvation Dynamics in Supercritical CO_2. *J. Chem. Phys.* **2006**, *124*, 044505.

(19) Ando, R. A.; Borin, A. C.; Santos, P. S. Saturation of the Electron-Withdrawing Capability of the NO_2 Group in Nitroaromatic Anions: Spectroscopic and Quantum-Chemical Evidence. *J. Phys. Chem. A* **2007**, *111*, 7194−7199.

(20) Hidalgo, M.; Rivelino, R.; Canuto, S. Origin of the Red Shift for the Lowest Singlet $\pi \rightarrow \pi^*$ Charge-Transfer Absorption of *p*-Nitroaniline in Supercritical CO_2. *J. Chem. Theory Comput.* **2014**, *10*, 1554.

(21) Millefiori, S.; Favini, G.; Millefiori, A.; Grasso, D. Electronic Spectra and Structure of Nitroanilines. *Spectrochim. Acta. A* **1977**, *33*, 21−27.

(22) Sigman, M. E.; Lindley, S. M.; Leffler, J. E. Supercritical Carbon Dioxide: Behavior of T* and P Solvatochromic Indicators in Media of Different Densities. *J. Am. Chem. Soc.* **1985**, *107*, 1471−1472.

(23) Sok, S.; Willow, S. Y.; Zahariev, F.; Gordon, M. S. Solvent-Induced Shift of the Lowest Singlet $\pi \rightarrow \pi^*$ Charge-Transfer Excited State of p-Nitroaniline in Water: An Application of the TDDFT/EFP1Method. *J. Phys. Chem. A* **2011**, *115*, 9801−9809.

(24) Kosenkov, D.; Slipchenko, L. V. Solvent Effects on the Electronic Transitions of p-Nitroaniline: A QM/EFP Study. *J. Phys. Chem. A* **2011**, *115*, 392−401.

(25) Eriksen, J. J.; Sauer, S. P. A.; Mikkelsen, K. V.; Christiansen, O.; Jensen, H. J. A.; Kongsted, J. Failures of TDDFT in Describing the Lowest Intramolecular Charge-Transfer Excitation in Para-Nitroaniline. *Mol. Phys.* **2013**, *111*, 1235−1248.

(26) Frutos-Puerto, S.; Aguilar, M. A.; Galvan, I. F. Theoretical Study of the Preferential Solvation Effect on the Solvatochromic Shifts of para-Nitroaniline. *J. Phys. Chem. B* **2013**, *117*, 2466.

(27) Day, P. N.; Pachter, R.; Nguyen, K. A. Analysis of Nonlinear Optical Properties in Donor-Acceptor Materials. *J. Chem. Phys.* **2014**, *140*, 184308.

(28) Cardenuto, M. H.; Coutinho, K.; Cabral, B. J. C.; Canuto, S. Electronic Properties in Supercritical Fluids: the Absorption Spectrum of *p*-Nitroaniline in Supercritical Water. *Adv. Quantum Chem.* **2015**, *71*, 323−339.

(29) Kovalenko, S. A.; Schanz, R.; Farztdinov, V. M.; Hennig, H.; Ernsting, N. P. Femtosecond Relaxation of Photoexcited Para-Nitroaniline: Solvation, Charge Transfer, Internal Conversion and Cooling. *Chem. Phys. Lett.* **2000**, *323*, 312−322.

(30) Coutinho, K.; Canuto, S. Solvent Effects from a Sequential Monte Carlo-Quantum Mechanical Approach. *Adv. Quantum Chem.* **1997**, *28*, 89−105.

(31) Marx, D.; Hutter, J. *Ab Initio Molecular Dynamics*; Cambridge University Press: New York, 2009.

(32) *A Primer in Density Functional Theory*; Fiolhais, C., Nogueira, F., Marques, M. A. L., Eds.; Springer: New York, 2003.

(33) Grimme, S. Semiempirical Hybrid Density Functional with Perturbative Second-Order Correlation. *J. Chem. Phys.* **2006**, *124*, 034108.

(34) Goerigk, L.; Moellmann, J.; Grimme, S. Computation of Accurate Excitation Energies for Large Organic Molecules with Double-Hybrid Density Functionals. *Phys. Chem. Chem. Phys.* **2009**, *11*, 4611−4620.

DOI: 10.1021/acs.jpca.6b01797
J. Phys. Chem. A 2016, 120, 3878−3887

(35) Karton, A.; Tarnopolsky, A.; Schatz, G. C.; Martin, J. M. L. Highly Accurate First-Principles Benchmark Data Sets for the Parametrization and Validation of Density Functional and Other Approximate Methods. Derivation of a Robust, Generally Applicable, Double-Hybrid Functional for Thermochemistry and Thermochemical Kinetics. *J. Phys. Chem. A* **2008**, *112*, 12868−12886.
(36) Becke, A. D. Density-Functional Termochemistry. III. The Role of Exact Exchange. *J. Chem. Phys.* **1993**, *98*, 5648.
(37) Lee, C.; Yang, W.; Parr, R. G. Development of the Colle-Salvetti Correlation-Energy Formula into a Functional of the Electron Density. *Phys. Rev. B: Condens. Matter Mater. Phys.* **1988**, *37*, 785.
(38) Risthaus, T.; Grimme, S. Benchmarking of London Dispersion-Accounting Density Functional Theory Methods on Very Large Molecular Complexes. *J. Chem. Theory Comput.* **2013**, *9*, 1580−1591.
(39) Woon, D. E.; Dunning, T. H. Gaussian Basis Sets for Use in Correlated Molecular Calculations. III. The Atoms Aluminum through Argon. *J. Chem. Phys.* **1993**, *98*, 1358.
(40) Hirata, S.; Head-Gordon, M. Time-Dependent Density Functional Theory within the Tamm-Dancoff Approximation. *Chem. Phys. Lett.* **1999**, *314*, 291−299.
(41) Neese, F. The ORCA Program System. *WIREs Comput. Mol. Sci.* **2012**, *2*, 73−78.
(42) Stanton, J. F.; Bartlett, R. J. The Equation of Motion Coupled-Cluster Method - a Systematic Biorthogonal Approach to Molecular-Excitation Energies, Transition-Probabilities, and Excited-State Properties. *J. Chem. Phys.* **1993**, *98*, 7029−7039.
(43) Christiansen, O.; Koch, H.; Jørgensen, P. The Second-Order Approximate Coupled Cluster Singles and Doubles Model CC2. *Chem. Phys. Lett.* **1995**, *243*, 409−418.
(44) Turney, J. M.; Simmonett, A. C.; Parrish, R. M.; Hohenstein, E. G.; Evangelista, F. A.; Fermann, J. T.; Mintz, B. J.; Burns, L. A.; Wilke, J. J.; Abrams, M. L.; et al. Psi4: an Open-Source Ab Initio Electronic Structure Program. *Wiley Interdisciplinary Reviews: Computational Molecular Science* **2012**, *2*, 556−565.
(45) Martyna, G. J.; Tuckerman, M. E. A Reciprocal Space Based Method for Treating Long Range Interactions in Ab Initio and Force-Field Based Calculations in Clusters. *J. Chem. Phys.* **1999**, *110*, 2810.
(46) Lippert, G.; Hutter, J.; Parrinello, M. A Hybrid Gaussian and Plane Wave Density Functional Scheme. *Mol. Phys.* **1997**, *92*, 477.
(47) VandeVondele, J.; Krack, M.; Mohamed, F.; Parrinello, M.; Chassaing, T.; Hutter, J. Quickstep: Fast and Accurate Density Functional Calculations Using a Mixed Gaussian and Plane Waves Approach. *Comput. Phys. Commun.* **2005**, *167*, 103.
(48) Martiniano, H. F. M. C.; Galamba, N.; Cabral, B. J. C. Ab Initio Calculation of the Electronic Absorption Spectrum of Liquid Water. *J. Chem. Phys.* **2014**, *140*, 164511.
(49) Goedecker, S.; Teter, M.; Hutter, J. Separable Dual-Space Gaussian Pseudopotentials. *Phys. Rev. B: Condens. Matter Mater. Phys.* **1996**, *54*, 1703.
(50) Vandevondele, J.; Hutter, J. Gaussian Basis Sets for Accurate Calculations on Molecular Systems in Gas and Condensed Phases. *J. Chem. Phys.* **2007**, *127*, 114105.
(51) Bussi, G.; Donadio, D.; Parrinello, M. Canonical Sampling through Velocity Rescaling. *J. Chem. Phys.* **2007**, *126*, 014101.
(52) Tomasi, J.; Mennucci, B.; Cammi, R. Quantum Mechanical Continuum Solvation Models. *Chem. Rev.* **2005**, *105*, 2999−3094.
(53) Chirlian, L. E.; Francl, M. M. Atomic Charges Derived from Electrostatic Potentials - a Detailed Study. *J. Comput. Chem.* **1987**, *8*, 894−905.
(54) Møller, C.; Plesset, M. S. Note on an Approximation Treatment for Many-Electron Systems. *Phys. Rev.* **1934**, *46*, 618−622.
(55) Cabral, B. J. C.; Rivelino, R.; Coutinho, K.; Canuto, S. A First Principles Approach to the Electronic Properties of Liquid and Supercritical CO_2. *J. Chem. Phys.* **2015**, *142*, 024504.
(56) Frisch, M. J.; Trucks, G. W.; Schlegel, H. B.; Scuseria, G. E.; Robb, M. A.; Cheeseman, J. R.; Scalmani, G.; Barone, V.; Mennucci, B.; Petersson, G. A. et al. Gaussian09 Revision A.02. Gaussian Inc.: Wallingford CT, 2009.
(57) Yanai, T.; Tew, D.; Handy, N. A New Hybrid Exchange-Correlation Functional Using the Coulomb-Attenuating Method (CAM-B3LYP). *Chem. Phys. Lett.* **2004**, *393*, 51−57.
(58) Jacquemin, D.; Le Bahers, T.; Adamo, C.; Ciofini, I. What is the "Best" Atomic Charge Model to Describe Through-Space Charge-Transfer Excitations? *Phys. Chem. Chem. Phys.* **2012**, *14*, 5383−5388.
(59) *MARCHES*; http://www.sciences.univ-nantes.fr/CEISAM/erc/marches/?p=973. (Accessed, January 2016).
(60) Kamlet, M. J.; Kayser, E. G.; Eastes, J. W.; Gilligan, W. H. Hydrogen Bonding by Protic Solvents to Nitro Oxygens. Effects on Electronic Spectra of Nitroaniline Derivatives. *J. Am. Chem. Soc.* **1973**, *95*, 5210−5214.
(61) Oka, H.; Kajimoto, O. UV Absorption Solvatochromic Shift of 4-Nitroaniline in Supercritical Water. *Phys. Chem. Chem. Phys.* **2003**, *5*, 2535−2540.
(62) Fujisawa, T.; Terazima, M.; Kimura, Y. Excitation Wavelength Dependence of the Raman-Stokes Shift of N,N-Dimethyl-p-Nitroaniline. *J. Chem. Phys.* **2006**, *124*, 184503.
(63) Fujisawa, T.; Terazima, M.; Kimura, Y. Solvent Effects on the Local Structure of p-Nitroaniline in Supercritical Water and Supercritical Alcohols. *J. Phys. Chem. A* **2008**, *112*, 5515−5526.
(64) Kavitha, E.; Sundaraganesan, N.; Sebastian, S. Molecular Structure, Vibrational Spectroscopic and HOMO, LUMO Studies of 4-Nitroaniline by Density Functional Method. *Indian J. Pure Appl. Phys.* **2010**, *48*, 20−30.
(65) Sinha, H. K.; Thomson, P. C. P.; Yates, K. Excited State Dipole Moments and Polarizabilities of Some Aromatic Alkenes and Alkynes. *Can. J. Chem.* **1990**, *68*, 1507.
(66) Sinha, H. K.; Yates, K. Effects of Positions of Donor and Acceptor Type Substituents on Ground- and Excited-State Charge Transfer: Electrochromism of Some Benzene Derivatives. *J. Am. Chem. Soc.* **1991**, *113*, 6062−6067.
(67) Wortmann, R.; Kraemer, P.; Glania, C.; Lebus, S.; Detzer, N. Deviations from Kleinman Symmetry of the Second-Order Polarizability Tensor in Molecules with Low-Lying Perpendicular Electronic Bands. *Chem. Phys.* **1993**, *173*, 99−108.

DOI: 10.1021/acs.jpca.6b01797
J. Phys. Chem. A 2016, 120, 3878−3887